BRNO UNIVERSITY OF TECHNOLOGY

VYSOKÉ UČENÍ TECHNICKÉ V BRNĚ

FACULTY OF ELECTRICAL ENGINEERING AND COMMUNICATION

FAKULTA ELEKTROTECHNIKY
A KOMUNIKAČNÍCH TECHNOLOGIÍ

DEPARTMENT OF RADIOENGINEERING

ÚSTAV RADIOELEKTRONIKY

TERAHERTZ ANTENNA ARRAYS FOR COMMUNICATIONS

TERAHERTZOVÁ ANTÉNNÍ POLE PRO KOMUNIKACI

SHORT VERSION OF DOCTORAL THESIS

ZKRÁCENA VERZE DIZERTAČNÍ PRÁCE

AUTHOR AUTOR PRÁCE	Dominika Warmowska, MSc. Eng.
SUPERVISOR ŠKOLITEL	prof. Dr. Ing. Zbyněk Raida

BRNO 2020

KEYWORDS

THz antenna arrays, microfabrication, micromachining, corporate-feed arrays, beam steering, high-gain antennas, circularly polarized antennas, antennas for space applications, thin metal modeling, THz antenna modeling, thin gold modeling.

BIBLIOGRAFICKÁ CITACE

STORAGE PLACE

Research department, FEEC BUT, Technická 3058/10, 602 00 Brno

TABLE OF CONTENT

INTRODUCTION

The dissertation thesis is focused on a design of circularly polarized terahertz antenna arrays for communications applications at THz frequencies. To make the thesis understandable, related topics are introduced in this chapter.

The first paragraph is conceived as an introduction to electromagnetic waves propagating at terahertz frequencies. Specific properties of those waves and their exploitation in selected applications are discussed. Attention is turned to wireless communication at terahertz frequencies and related losses.

Since in the THz range, the losses are significantly higher compared to microwave frequencies, antennas have to be designed to contribute to the compensation. Challenges of THz antenna fabrication technologies are given in the second paragraph.

Circularly polarized waves are preferred for communications, and therefore, circular polarization is discussed in the third paragraph of the Introduction.

The fourth paragraph is devoted to satellite communications technologies, the recent advancements and challenges, and requirements on antennas for satellite communications.

1.1   THZ AND SUB-THZ WAVES

Terahertz (THz) radiation is an electromagnetic radiation in the spectrum of frequencies ranging from 0.1 THz to 10 THz which correspond to wavelengths from 3 mm to 30 μm. Waves within the lower range of the THz band, 100 GHz – 300 GHz, can sometimes be referred to as sub-THz waves.

The position of the THz band in the electromagnetic spectrum is shown in Figure 1. The THz band is still not well explored, when compared to relatively well-developed science and technology in the microwave and optical parts of the electromagnetic spectrum.
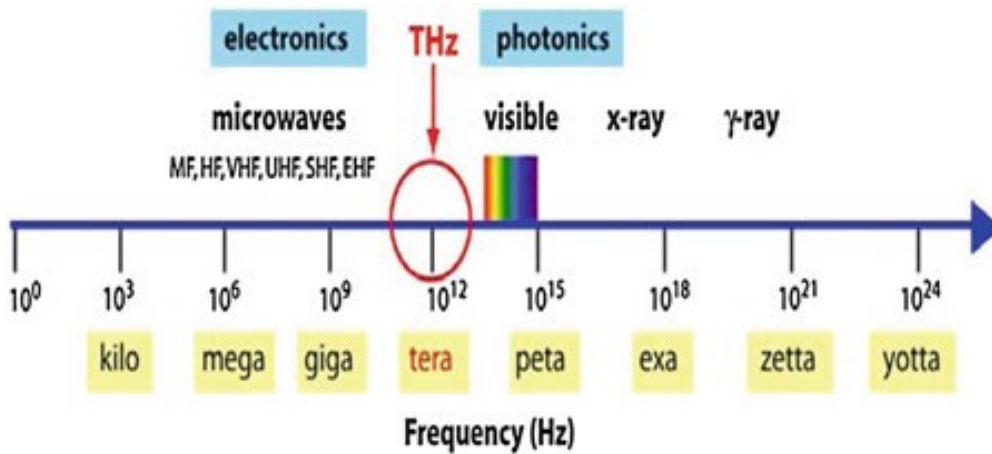
Figure 1. Position of the THz band in the electromagnetic spectrum [1].

The THz radiation has many interesting properties which differ from other waves in the electromagnetic spectrum.

The presented characteristics of THz waves differ from waves in different ranges of the electromagnetic spectrum. Thanks to the unique features, there are many applications which exploit devices and systems operating in the THz range:

- **Communications.** In recent years, the demands for high data rates and wide bandwidth of wireless communication have dramatically increased. In order to achieve high data rates of 10 to 20 Gbit/s, the carrier frequencies in the millimeter or sub-millimeter wavelengths range are necessary to be used. The attenuation at THz frequencies is high, but there are several bands that could be used for high-data-rate wireless communication.

- **Medical Imaging.** Water has a high absorption in the THz spectrum. Therefore, hydrate objects exhibit a strong contrast in comparison with surrounding materials. The THz radiation is quite gentle to the human body due to the high water absorption, and THz waves cannot penetrate into the human body.

Current demand on data transfers is constantly rapidly increasing, and high-performance THz antennas are necessary. Therefore, this work focuses on developing THz antennas for communication systems.

1.1.1 Transmission losses at THz frequencies

Although the THz waves have a lot of interesting and useful characteristics, there are some challenges in exploiting this part of the electromagnetic spectrum. There are three types of losses related to an electromagnetic wave transmission [2].

First, the strong atmospheric attenuation occurs at THz frequencies.

Second, the free space path loss (FSPL) is the source of losses in the THz region.

Lastly, high losses in the THz region are related to the non-line of sight propagation. This propagation occurs when there are objects in the Fresnel zone of the communicating antennas.

Since the losses in the THz region are higher than losses at lower frequencies, THz antenna designs need to contribute to their compensation. Hence, the antennas should provide a high gain and very directive radiation characteristics. Moreover, the distances on which the communication systems are operating have to be much smaller than for low-frequency systems.

1.2 CIRCULAR POLARIZATION

One of the biggest advantages of the circularly polarized antennas is that they do not require alignment of the transmitting and the receiving antenna. Moreover, circularly polarized links benefit from resilience to multipath reflections in different environments as well as other propagation effects dependent on polarization such as Faraday rotation [3] and reduction of rain clutter [4].

Considering these advantages, circularly polarized antennas are preferred in communications systems to avoid unnecessary losses added to the transmission losses in the THz region. Circularly polarized antennas are widely employed in many different applications such as

terrestrial communication systems, satellite communication systems, radars [5] and others.

1.3   BEAM STEERING

As it was already stated, at THz frequencies the channel losses are considerably higher than at the microwave range. One of the solutions to those loses is beam forming which is related to employment of antennas with highly directive and narrow beams.

Moreover, in order to localize and communicate with the mobile terminals, beam steering is necessary. By choosing the proper direction of radiation, the unwanted signals can be avoided for the receiving antenna and in case of transmitting antenna the beam can be steered in the direction of the receiving terminal. Currently, the most popular solution to achieve beam steering is implementing active phase shifters in the antenna feeding. However, the complexity is high which is related to high digital demand, large size as well as increased temperature of the devices [2]. Passive phase shifters offer interesting characteristics [6]–[8] without the disadvantages that the active ones hold [2].

1.4   SATELLITE COMMUNICATIONS

Currently, SatComs operate mainly in L, S and C bands. Applications such as GPS, Galileo, weather and ship radars, SatComs, space research, space operation, EO satellite services, TV broadcasting are all using the spectrum within the L, S and C bands [9]. Those bands spread across 1 to 8 GHz, and altogether provide only 7 GHz bandwidth. Therefore, the existing frequency bands become congested. Bandwidth is abundant in the higher frequencies ranges and the transition of the satellite technologies to those bands is unenviable. Hence, new communication systems, including antennas, with excellent parameters, operating at the K and Ka bands are necessary. The satellite spectrum with the most exploited bands L, S, and C and future bands K, Ka, and Q/V is presented in Figure 2 [9].
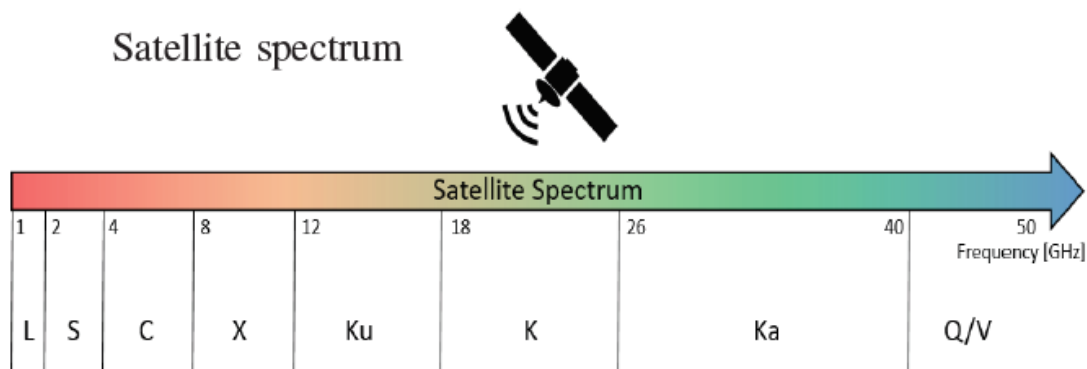
Figure 2. Satellite spectrum [9].

2   STATE-OF-THE-ART

The content of this chapter is a brief introduction to THz antennas and THz antennas designed for communications. Next, designs of antennas for satellite communications are presented. The following paragraph is devoted to the modeling of thin metallic structures at THz frequencies. In the last paragraph, the advances in microfabrication technologies are given.

2.1   THZ ANTENNAS

2.1.1 THz antennas for communications

Fabry-Perot antennas [10]–[12] antennas can radiate circularly polarized signals, have a low profile, and, thanks to a large number of radiating elements, can achieve high gains. However, their bandwidths are very limited (1-3%) and the design proves to be very problematic to be scaled to THz frequencies, mostly due to fabrication limitations.

Lens antennas can overcome all the previous challenges by placing spiral (or other planar antennas) on a dielectric lens. However, these lenses should be electrically large in order of $10\lambda_0$ [13].

Dielectric rod waveguide antennas achieve excellent gains and bandwidths. However, they have an electrically large height [14]–[17]. A similar issue occurs for the horn antennas that were discussed before.

The large size of the lens, horn, and dielectric rod antennas can make it problematic to integrate them into modern communication systems. Therefore, a compact high gain and circularly polarized solution with a straight-forward manufacturing process is necessary.

On the other hand, **corporate feed antennas** can be integrated into the system easily. These types of antennas usually include multiple layers comprising radiating elements (slots or patches) and feeding networks which excite radiating elements. Even though these antenna structures consist of many layers, the profile of corporate feed arrays is very low, as all the layers have a small height. By increasing the number of radiating elements in the array, the gain is increased, the radiation pattern becomes more directive, and the bandwidth is enhanced [18]. Therefore, corporate feed arrays are a promising solution for creating a high gain, wide bandwidth THz antennas.

In [19], the authors presented multilayered 2×2 and 4×4 arrays. The antennas were designed and manufactured to operate at 1 THz. One of the manufacturing steps included a spin coating by a photoresist of the thickness of $\lambda/4$, which is very thick at lower THz frequencies, and therefore problematic to manufacture. The presented design was compact and wideband, however, the gain was limited to 10 dBi (the 2×2 array) and14 dBi (the 4×4 array). Moreover, the antennas did not provide circular polarization.

In [20], the authors presented a larger array with a similar design to be operated at 350 GHz. Also, a silicon-based manufacturing process was included, and the antenna achieved a higher gain. However, the antenna [20] was again designed for linear polarization and had an electrically large height.

Another antenna with slot radiators and the corporate feed was presented in [21]. The antenna

operated at 60 GHz, showed high-gain and radiated circularly polarized waves. Nevertheless, the bandwidth was only 4% and the design with multiple thin layers is not feasible to be implemented at THz frequencies.

2.1.2 Antennas with beam steering capabilities

One of the conventional ways in order to achieve beam steering in the required direction is the mechanically move the antenna. This solution is employed in radar systems, however it is not suitable for modern communications applications, because of high time consumption, latency requirements and large sizes.

Frequency scanning antennas, do not require the use of phase shifters or mechanical steering and can achieve high range of steering angles. Many implementations of frequency scanning antennas at THz frequencies have been presented [22]–[24]. However in such solutions the beam steering is never obtained at single frequency, the beam direction changes with the varying frequency.

Currently, antennas with active phase shifters are widely used because of their impressive parameters. THz antennas with beam steering implemented by active phase shifters were presented in [25], [26]. However these phase shifters have high digital demands and complexity which has a direct influence on their cost and size [9].

In [27] authors present a dielectric rod antenna array with liquid crystal phase shifters that allow beam reconfigurability. However, the antenna operates only at 100 GHz and can steer the beam into three different directions. Another antenna employing liquid crystal phase shifters in a Fabry-Perot cavity was described in [28]. The antenna operates at 1 THz, however the beam cannot be continuously steered. Presented THz beam steering antennas offer interesting characteristics, however none of them has the ability to continuously steer the beam, has high gain and operates with circular polarization.

2.2 ANTENNAS FOR SATELLITE COMMUNICATIONS

Currently, the SatComs research is focused on improving the capabilities of the communication links to increase the data rates and deliver coverage to underserved areas [9]. To achieve that, an antenna design with high gain and wide bandwidth is necessary. The main challenges for the antenna designers are to improve the gain and bandwidth while fitting within the size, power, and weight limits for Satellite Communications.

One of the most common solutions for high-gain space missions antennas are deployable reflector antennas [29]. Although they enable the multiple-frequency operation with high efficiency and high gain, they still require high mechanical complexity due to their deployment. In [30], an inflatable antenna was presented, which also provides high gain, but the bandwidth is achieved in Ka-band is only 0.5%. Additionally, it has a complex structure as it needs to be filled with gas.

As another solution, the authors presented in [31] is a Ka-band helical antenna. However, it has a gain of only 21 dBi and of 25 λ_0. A metallic antenna with a high-gain and wide bandwidth was presented in [32], it achieves pick gain of 26 dBi with the size of 7×7 λ_0. An advantage of such antenna is a lack of an unreliable deployment or inflation mechanism.

2.3   MICROFABRICATION TECHNOLOGIES

Two manufacturing technologies enable micromachining, and thanks to them innovative antennas, detectors, sensors and other devices can be manufactured, these technologies are dry etching and bonding.

2.3.1 Dry Etching

Etching allows controlled removal of desired material from a substrate. Etching methods can be primarily divided into two categories: wet etching and dry etching. Wet etching is referred to as etching the substrate by a liquid chemical. Dry etching is etching the material by gases or plasmas, where the main etching mechanism can be fully chemical, fully mechanical or mix of the two [33].

Deep Reactive Ion Etching (DRIE) is especially useful for antenna manufacture, because almost straight vertical walls can be obtained. DRIE has the advantage of anisotropic etching thanks to passivation of the vertical walls, which protects them from etching gases. The results of two types of DIRE: Bosch and cryogenic processes are presented in Figure 3.
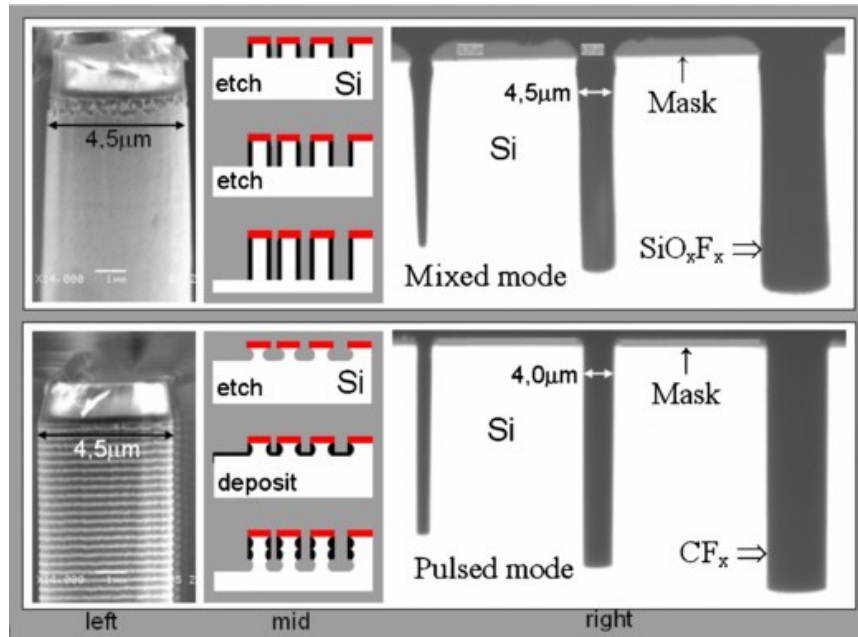
Figure 3. Comparison of results of deep reactive ion etching in mixed mode (cryogenic process) and pulsed mode (Bosch process) [34].

Cryogenic etch is one of the DRIE methods. This process is a mixed-mode etch when etching gasses and passivation gasses are released simultaneously. The etching includes the use of SF_6 and O_2, the gases mix and SiO_xF_y grows on the walls providing passivation for them and F_x etches the silicon. This type of etching is predominantly chemical etching. The advantage of this method is that the gases used are clearer than in the Bosch method and the vertical walls are much smoother. However, in order for the passivation layer not to evaporate the process has to take place in temperature from -140°C and -85°C. Moreover, because the same gas is responsible for etching as well as passivation, the process outcomes are harder to control [35], [36].

Bosch etch is another method of DRIE. This process is a pulsed mode etch where for a short period an etching gas is released then stopped, after that a passivation gas is released for walls passivation and stopped, in such a way the process is continued until the required number of iterations is reached. SF_6 is used as an etching gas here and C_4F_8 as a passivation gas. In case of Bosch process, the etching is predominantly mechanical, based on milling. The presence of two gases where each of them is responsible for etching or passivation allows better control of the process in comparison to the cryogenic etch. Moreover, the fact that the process can be done in temperature around 15° C and does not need intensive cooling down is another advantage of this process [34].

2.3.2 Bonding

Bonding is a process of fixing two wafers together with high alignment and is usually used in the packaging of electronics. Wafer bonding can be divided into bonding with intermediate layer and direct bonding.

Bonding is an enabling technology for micromachining. During antenna manufacture bonding tends to be used to fix together layers of a multilayer structure with good accuracy. Usually, bonding is the last step of the antenna manufacture, therefore the surface is not extremely smooth anymore, for this reason, bonding with intermediate layer is preferred.

3   OBJECTIVES

The dissertation thesis is focused on a design of a **circularly polarized terahertz antenna array**. To make the design comprehensive:

- The physical behavior of metallic surfaces at THz frequencies has to be properly modeled. Hence, **comparison of modeling approaches to be used for metallic surfaces** of THz antenna arrays is the first objective.

- An **antenna suitable for communications in the THz range** should be designed. To be suitable for THz communications applications, the antenna should be circularly polarized, have high gain, wide axial ratio bandwidth and directive radiation. Developing the design methodology is the second objective.

  The design methodology should comprise the possibility to extend the antenna to a bigger array. When completed by phase shifters, the array should be capable to steer the main beam. Moreover, the design technology should allow the array to be manufactured by a microfabrication technology.

- Properties of fabrication technologies have to be considered when modeling the array. Hence, technologies for manufacturing THz arrays have to be compared and **the designed antenna at THz frequencies should be manufactured by microfabrication** technologies, which is the third objective.

  The best available technology is chosen, and different THz constraints and phenomena are taken into consideration. Technological aspects are considered when modeling.

- The **design procedure should be as general as possible,** which is the fourth objective. The generality of the procedure is verified by replicating the design at microwave frequencies.

  The replication resulted in a circularly polarized antenna array suitable for space applications. Attention is turned to high gain, wide axial ratio bandwidth, low-profile and performance better than state-of-art antenna designs provide.

4   MODELING METAL AT THZ FREQUENCIES

At lower frequencies, the electromagnetic field can be assumed to rapidly decay in a metal, and the metallic surface can be approximated by a perfect electric conductor with a relatively small deviation from reality.

At terahertz frequencies, behavior of metals significantly changes. The depth of electromagnetic wave penetration and the thickness of used metallization layers influences the conductivity. Such an effect has to be taken into consideration in the numerical model.

For the proper modeling of different structures with thin gold layers at THz frequencies, the relationship between the thickness of the gold layer and the conductivity is discussed in detail. Test models were created in HFSS and CST Microwave Studio.

In the case of the time-domain finite-integration technique (CST Microwave Studio):

- Default options (no additional boundary conditions were associated with a thin gold layer).

In the case of the frequency-domain finite-element technique (HFSS), different methods have been considered:

- Default options (no additional boundary conditions were associated with a thin gold layer),
- Meshing inside the gold layer,
- *Finite Conductivity* boundary was applied,
- *Layered Impedance* boundary was associated.

In addition to the two main models including the default modeling in CST and HFSS simulators, three other models were tested.

As a proof of concept for showing the effect of different simulation models, a metallic waveguide with an internal thin metal wall was studied. For the simulations, a waveguide that provides a single-mode TE_{10} performance at the frequency of interest was employed. At 350 GHz the used waveguide was WR 2.2 with dimensions of 0.570 mm × 0.285 mm.

The waveguide was terminated by a wave port to act as a matched load. An internal thin metallic wall, with the same cross-section as the waveguide, was placed in the center of the waveguide. The thickness of the gold layer varied in a range from 0.01 μm to 10 μm. The model that was used is depicted in Figure 4. The skin depth of gold on tested frequency is $\delta = 132$ nm.

11
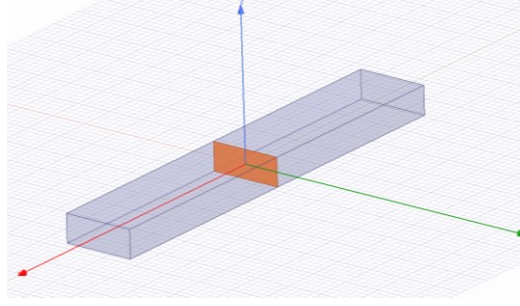
Figure 4. Model of the waveguide with a thin gold sheet inside.

For comparison purposes, the theoretical calculations of the reflection coefficient were also performed following [37].

In Figure 5 the reflection coefficient at the input port of the waveguide is depicted as a function of the gold-layer thickness using the previously discussed methods at testing frequency 350 GHz.
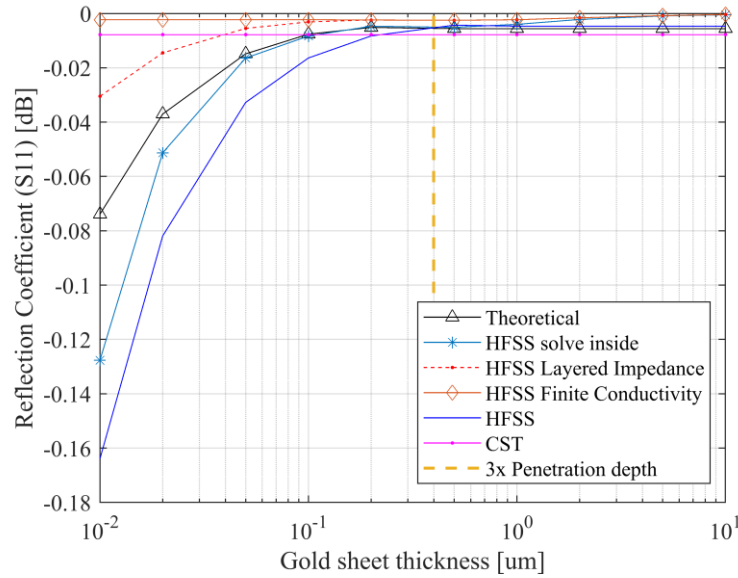
Figure 5. Reflection coefficient at the input port of waveguide as a function of the thickness of a gold wall in the cross-section at 350 GHz.

After analyzing the results at 200 GHz, 350 GHz and 500 GHz it was concluded that acceptable outputs are obtained if the gold layer thickness is:

- Lower than 3 δ (HFSS layered impedance or solve inside);
- Higher than 3 δ (all expect HFSS with solving inside).

Considering these conclusions, conditions at the boundary of the gold and the air can be efficiently modeled depending on the operation frequency and the thickness of the gold layer.

5 CORPORATE FEED THZ ANTENNA DESIGN AND MODELING

In this chapter, a design of a THz antenna array for communications is presented. The design methodology is given, including the design of the 2×2 array element and 4×4 antenna array. The simulation results of both the antennas are given and compared with state-of-the-art structures.

Models of THz antennas with thin metallic walls incorporating different boundary conditions and different material structure are analyzed and compared. The best modeling strategies are chosen. Sensitivity analyses are performed prior to fabrication. In the last sub-chapter a beam steering capability of the designed antenna is discussed.

5.1 Design methodlgy

In this sub-chapter, the design considerations are discussed. Then, the design of an array element is presented. The design procedure and dimensions considerations for the 2×2 are further discussed. The array element is designed in the way to enable expansion it into a larger array, which is represented by a 4×4 array design. The simulation results of both of the antennas are presented and pre-manufacture analyses are performed. Finally, the designed antennas are compared with state-of-the-art antenna designs.

The objective of the presented design is to achieve an antenna that shows a directive radiation with a high gain, radiates circularly polarized wave, operates in wide impedance and polarization bandwidth, and works at THz frequencies. The design should enable antenna elements to be grouped into a multiple-element antenna array. Moreover, current manufacturing possibilities and constraints have to be taken into consideration.

5.1.1 Antenna design

The antenna array element design consists of four radiating elements and it is fed from a single point of the feeding system. Antenna element is designed in a way that enables further expansion to an array consisting of multiple antenna elements. The multilayer design is fully based on air-filled metalized waveguides, slots and cavities. The design is prepared to operate at a central frequency of 350 GHz. The design of the antenna elements is presented in Figure 6.
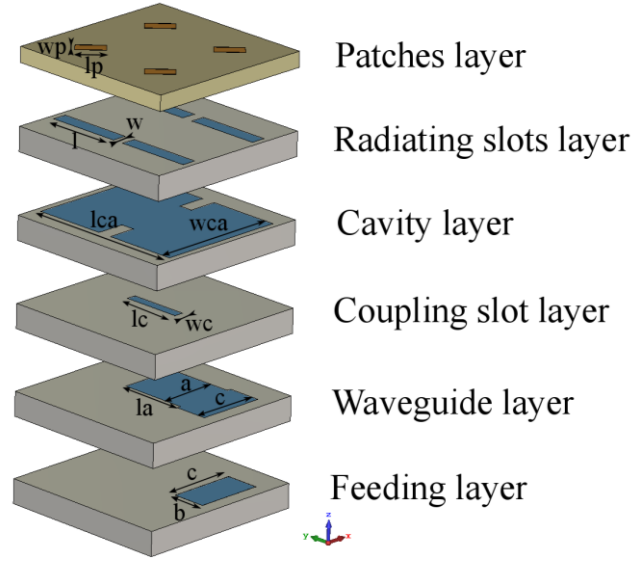
Figure 6. The 2x2 antenna element.

The signal is to fed to the antenna from the bottom through a WR2.2 waveguide. For this reason, the bottom layer – the feeding layer has a slot with the size identical to the size of a WR2.2 waveguide. The feeding layer and the waveguide layer create an E-bend transmission.

The waveguide layer includes a part of a waveguide, this layer is extended to a feeding system when the array is enlarged. In the waveguide, the fundamental mode TE_{10} is excited by the port. EM field in the waveguide is coupled to upper layers by the coupling slot.

The signal from the waveguide is coupled to the cavity by the coupling slot. The slot is a shunt slot, positioned longitudinally in the end-left corner of the waveguide to couple the maximum power to the cavity. All the five bottom layers have the same thickness of $t = 0.2$ mm.

The coupling slot is located centrally with respect to the cavity. In the cavity, the iris walls ensure the required field distribution and appropriate impedance matching. The simulated electric and magnetic field distribution in the air-filled cavity is shown in Figure 7. The central-plane of the cavity along the y-axis is equivalent to an electric wall. Therefore, the direction of the field in the right part of the cavity is opposite to the field in the left part of the cavity. Thanks to this, four slots can be excited not only with the same amplitude but also in-phase.
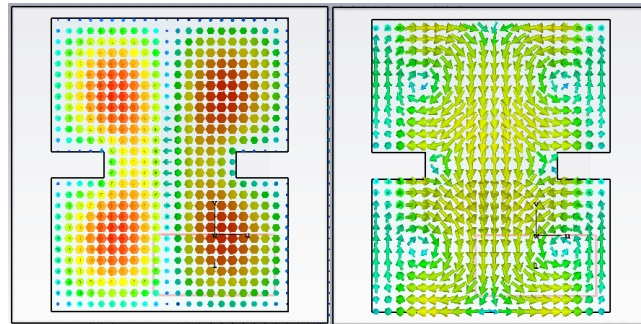

Figure 7. The electric (left) and magnetic (right) field distribution
in the cavity of the antenna element.

On top of the cavity, in the radiating slots layer, four rectangular slots are located.

The last layer is a dielectric layer made of Arlon CuClad 217 [38]. The dielectric layer has a height of $h = 0.127$ mm. On the top of the dielectric, metallic, rectangular patches are placed.

Each patch is rotated by 45° with respect to the radiating slot below. The power radiated by radiating slots excites metallic patches, and, because of the 45° rotation, two orthogonal modes are excited in each patch and the circular polarization is created. The mechanism of the circular polarization creation is presented by showing the surface current distribution on the patches in Figure 8.

The size of the antenna element (2×2 array) is $1.75\lambda_0 \times 1.75\lambda_0 \times 1.3\lambda_0$.
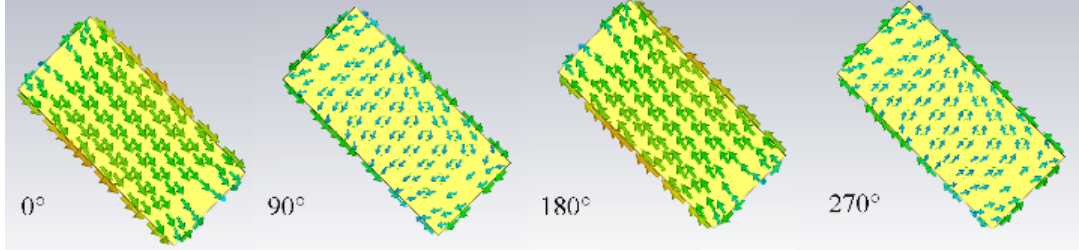
Figure 8. The surface current distribution on the patches in the top layer in phases: 0°, 90°, 180°, and 270°.

The 2×2 antenna element was expanded to the 4×4 array. The top layers were multiplied, and in the waveguide layer, a feeding system was introduced. This ensures an easy array expansion; only the feeding system needs to be designed.

5.1.2 Simulation results

The designed antenna element was simulated in CST Microwave Studio. Where the 2×2 array element achieves a peak of the realized gain for the left-handed circular polarization of 13.8 dBi, the 4×4 array achieves the value of 18.4 dBi.

Frequency responses of the reflection coefficient and realized gain for the left-handed circular polarization of the 4×4 and 2×2 antenna arrays are shown in Figure 9. The 2×2 antenna array operates in a frequency band of 25 GHz and the 4×4 antenna array in a frequency band of 30 GHz. Frequency bands are given for both impedance and polarization (related to axial ratio) bandwidths.
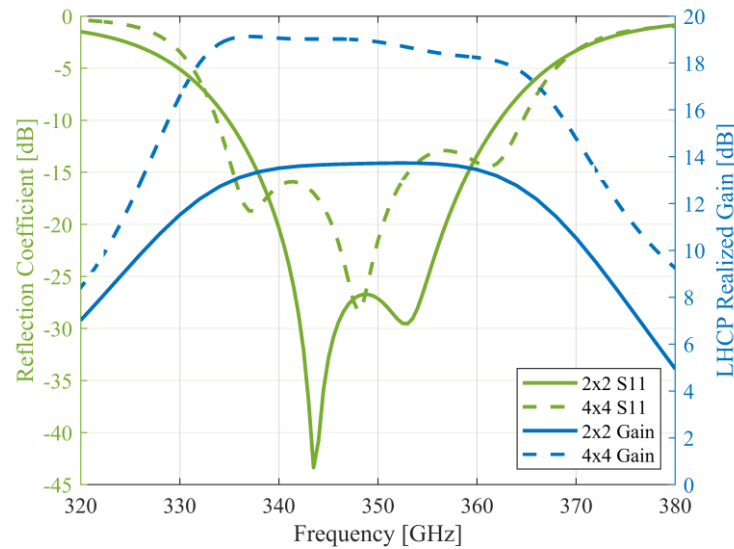
Figure 9. Simulated reflection coefficient and the left-handed circular polarization realized gain response vs frequency of the 2×2 and 4×4 antenna arrays.

The radiation efficiencies for both the 2×2 and the 4×4 antenna arrays are shown in Figure 10. In the operating band, the 2×2 antenna array has radiation efficiency above 0.90 and the 4×4 antenna array above 0.85. The presented efficiencies are given for the precise models that take into consideration all the metal and dielectric losses of materials (see more in the modeling chapter). However, models do not account for manufacturing inaccuracies (including over-etching and surface roughness). The efficiencies are expected to decrease for the fabricated antennas because of fabrication inaccuracies.
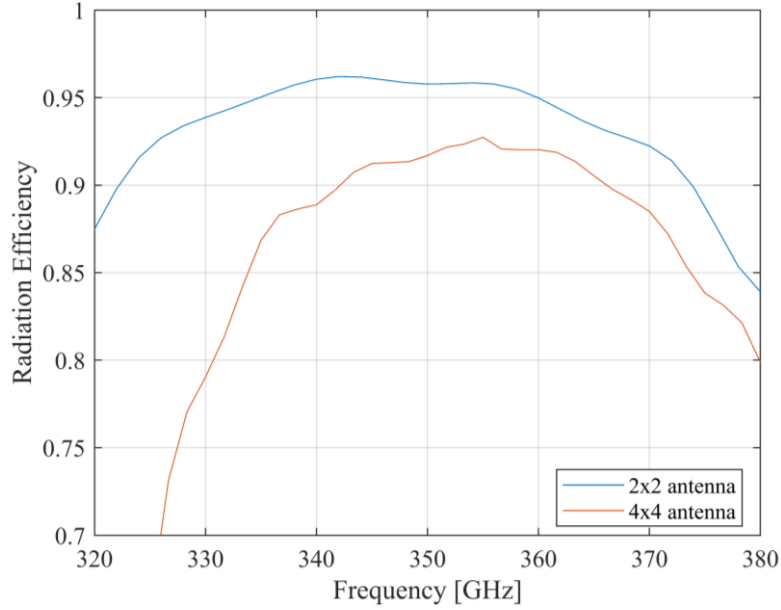
Figure 10. Simulated radiation efficiency of the 2×2 and 4×4 antenna arrays.
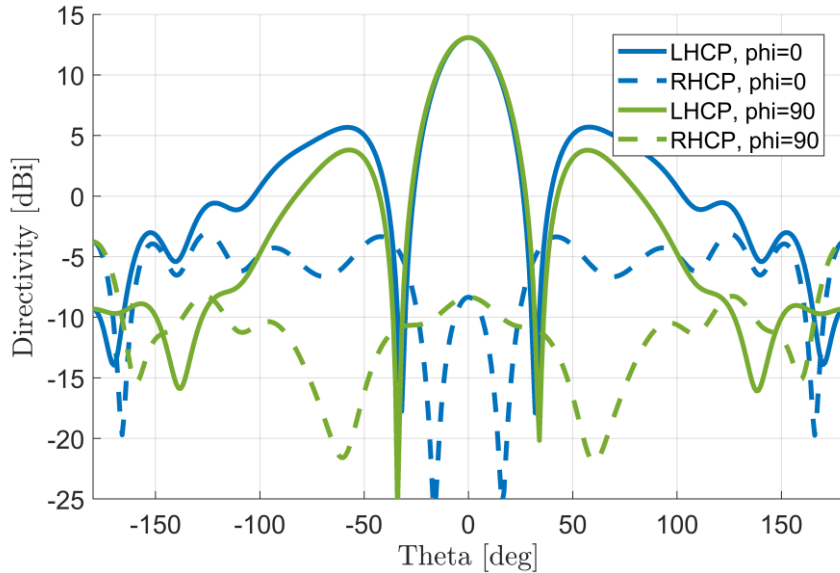
Figure 11. Simulated gain for θ = 0° and θ = 90° for the right-handed circular polarization (RHCP) and the left-handed circular polarization (LHCP).

The radiation patterns of the 2x2 antenna element for θ = 0° and for θ = 90° for the right-handed and left-handed circular polarization, are depicted in Figure 11. The antenna shows a highly directive radiation pattern, with front to back ratio of 24 dB. The isolation between co-

polar (LHCP) and cross-polar (RHCP) components at the boresight is higher than 35 dB.

Radiation patterns for θ = 0° and for θ = 90°, for the 4x4 antenna array at the bandwidth border frequencies (335 GHz and 365 GHz) and center frequency (350 GHz) for RHCP and LHCP are shown in Figure 12 and Figure 13.
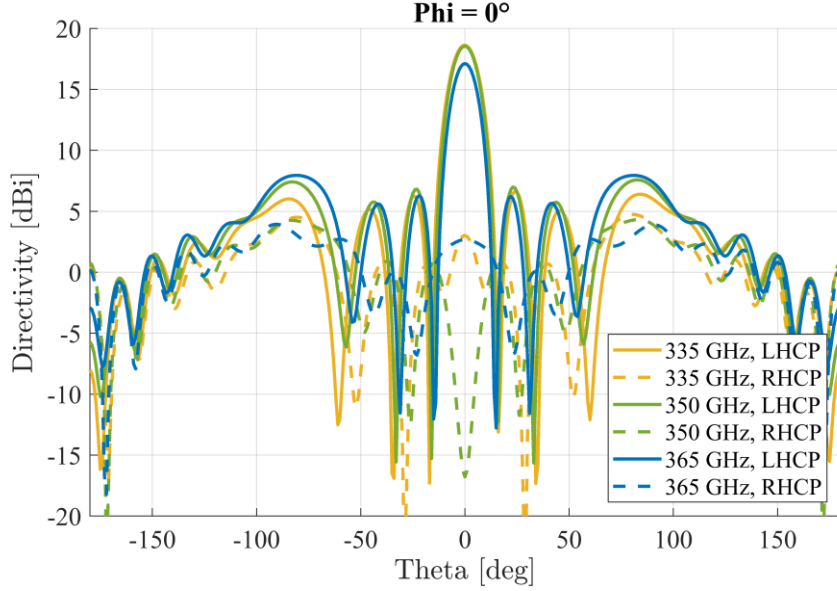
Figure 12. Directivity of the 4x4 antenna array for θ = 0°.
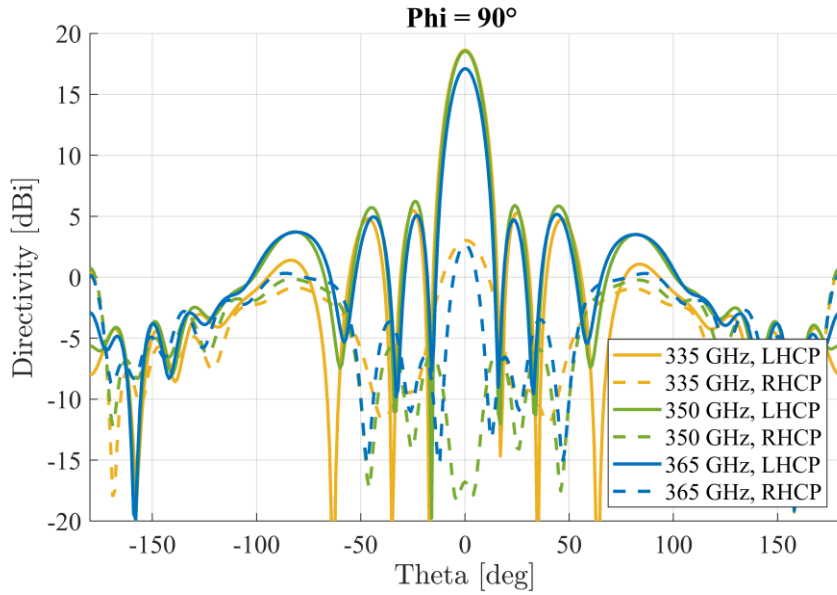
Figure 13. Directivity of the 4x4 antenna array for θ = 90°

5.1.3 Comparisons with state-of-art

In Table 1, comparison to other high-gain/circularly polarized antennas is given. The size is given as a diagonal in relation to λ_0. Most of the antennas present interesting results, however, none of them achieve simultaneously high-gain, circular-polarization, wide bandwidth, low profile, and THz operation (feasibility of fabrication the design at THz frequencies).

Table 1. Comparison of high-gain/circularly polarized/THz frequency antennas with this work. Operation frequency f_c, impedance bandwidth *BW*, and circular polarization *CP*.

Ref.	Design	f_c (GHz)	Height (λ_0)	Size (λ_0)	BW (%)	Max gain (dBi)	CP
[39]	Bow-tie	350	0.12	2.3	20	6	Y
[40]	Horn	340	8.4	4	12	20	N
[10]	Fabry-Perot	10	0.05	5.7	0.3	15	Y
[10]	Fabry-Perot	1000	0.006	4.2	1.4	12	Y
[12]	Fabry-Perot	15	0.85	9.9	2	19	Y
[41]	Conical spiral	8	4.5	5.7	150	10	Y
[14]	Dielectric Rod	61	4	4.1	2	15	Y
[13]	4 × 4 Lens	257	14	31.1	160	30	N
[16]	4 × 4 Dielectric Rod	92.5	20.6	4.3	38	23.5	N
[17]	Dielectric Rod	155	11	0.76	19	17.5	N
[19]	4 × 4 Met. posts array	1000	3	2.8	26	14	N
[20]	16 × 16 Slot array	350	7	18.1	13	30	N
[21]	16 × 16 Slot array	61.5	2	21.5	4	33	Y
This work	2 × 2 Slot array	350	1.3	2.5	8	13.8	Y
This work	4 × 4 Slot array	350	1.3	5	9	18.4	Y

5.2 MODELING OF THE THZ ANTENNA

The in-depth analysis of a terahertz antenna array with thin metallic walls is costly in terms of computational resources needed. A simplified analysis is necessary for quick, preliminary antenna design, and can be useful during the optimization. To demonstrate potential simplifications, different models of the 2×2 array were created.

High surface roughness and different thickness of the metallic layers can influence the antenna performance. Analyses of the significance of these parameters on antenna characteristics are needed.

Three different models of the 2×2 array were defined as:

- The PEC model.

- A full-gold model.

- The precise model of the antenna.

In Figure 14, three models are presented. Different materials were depicted by different colors: in beige the dielectric (Arlon CuClad 217), in orange copper, in grey PEC, in yellow gold and in pink silicon. The gold layer thickness in the precise model is not in scale for better visibility.
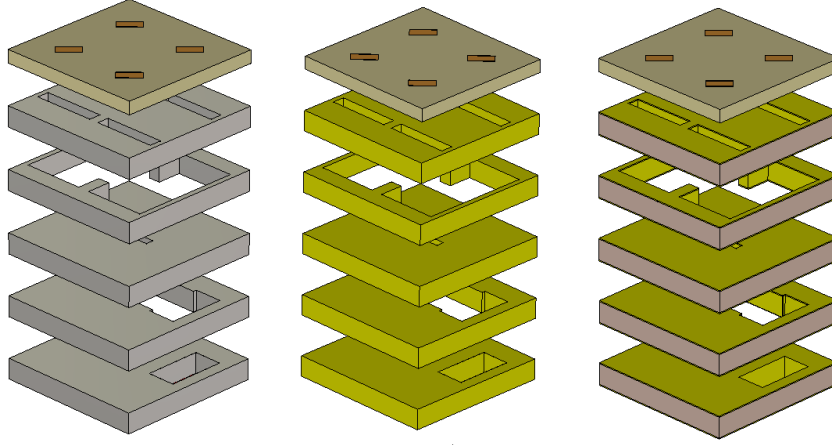
Figure 14. Three analyzed models of the antennas from the left: PEC model, full-gold model and precise model.

The models were analyzed in CST (time-domain finite-integration technique) and HFSS (frequency domain finite-element method).

Considering the accuracy of results and the computation time, the HFSS bulky-gold model produces results agreeing well with the reference model. For fine modeling, the HFSS bulky-gold model is recommended.

The PEC CST model is recommended to be used for fast and time-efficient calculations (a recommended choice for optimization). The antenna modeled this way can be fully characterized within the whole operating band in 2:41 minutes.

5.3 ANTENNA ARRAY WITH BEAM STEERING CAPABILITY

One of the ways to overcome the high losses in the THz region is the employment of beam steering. While the use of beamforming creates a very directive radiation pattern and enhances the gain, beam steering allows to switch the direction of the radiation of the antenna. By choosing the proper direction of radiation, the beam can be steered in the direction of the receiving terminal. In order to incorporate beam steering in an antenna array, it is necessary to include phase shifters in the feeding system.

5.3.1 Antenna design

Inspired by the impressive results mentioned before, the designed antenna array was extended to 8×8 elements to incorporate beam steering. The antenna design is presented in Figure 15. Liquid crystal, carbon nanotubes or MEMS phase shifters could be implemented in the antenna feeding layer to achieve phase shifting.
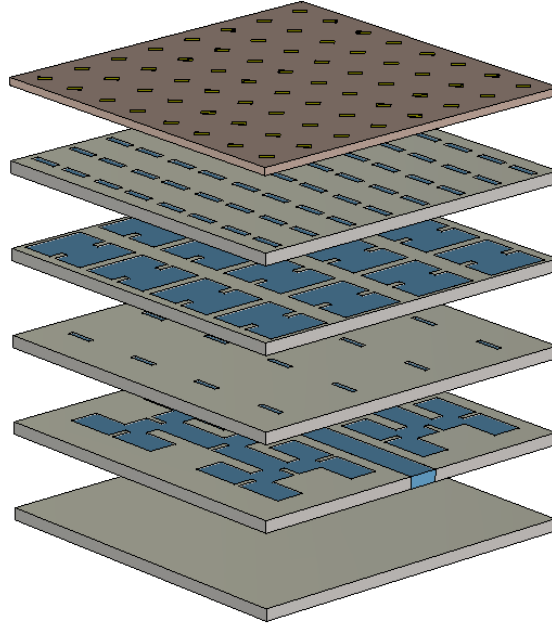
Figure 15. The 8×8 antenna with beam steering design capability.

The feeding system can be expanded in the same manner as for expansion from 2×2 to 4×4 array. Phase shifters could be placed into the feeding layer, which requires appropriate adjustments in this layer.

The feeding system has to be redesigned depending on the type of a phase shifter employed. Since the type of the phase shifter is unknown, the phase-shifting was introduced automatically in the signal fed through the coupling slots to simulate the antenna performance.

5.3.2 Simulation results

The phase shift is introduced in the feeding layer in a way that every column of coupling slots had a phase shift of +30° in relation to the previous column. In this way, each 2x2 antenna array element is fed by the signal with the same phase. By introducing such a progressive phase shift on each column of coupling slots, the azimuthal tilt of the beam was achieved, with the beam tilted by 2°. By increasing the progressive phase shift to 80°, the azimuthal tilt of 8° was obtained.

By changing the phase shift for every verse of coupling slots, scanning in elevation was achieved with the same maximum tilt of 8° for 80° progressive phase shift in each verse. The azimuthal scanning presented by radiation patterns in gain of the array with progressive phase shifts from -80° to 80° is shown in Figure 16. In such a manner, the beam can be tilted simultaneously both in azimuth and elevation.

The antenna radiates waves with left-handed circular polarization. The axial ratio and gain plots in frequency are presented in Figure 17 for the θ = 0° and main beam direction of 0°. The axial ratio bandwidth for each of the available beams between -8° to 8° in azimuth and elevation is at least 10 GHz, from 345 GHz to 355 GHz. The impedance bandwidth of the antenna is from 345 GHz to 355 GHz. The gain of the antenna is above 21 dBi in the whole bandwidth and for all beam directions.

These analyses prove that the antenna design is suitable for advanced beam steering

applications, with scanning in two dimensions, where a directive circularly polarized beam is radiated with very high gain and in a wide bandwidth.
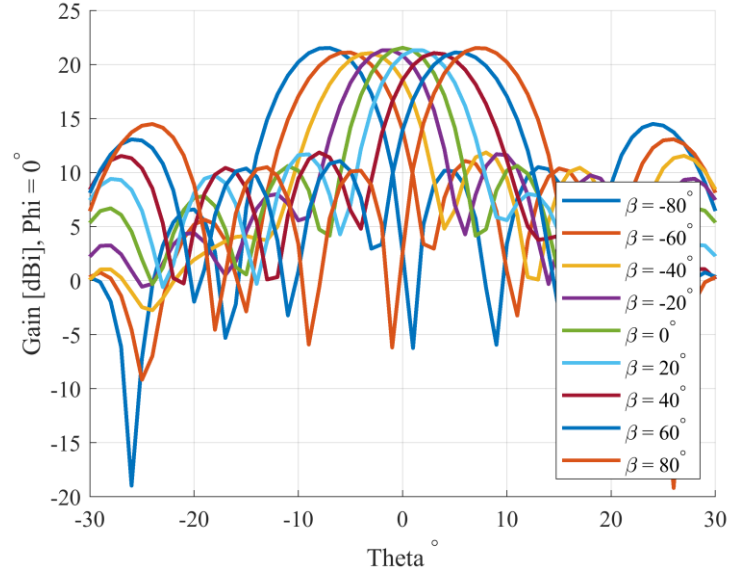
Figure 16. 8x8 antenna array directivity, θ = 0°, scanning in azimuth.
β describes the progressive phase shift.
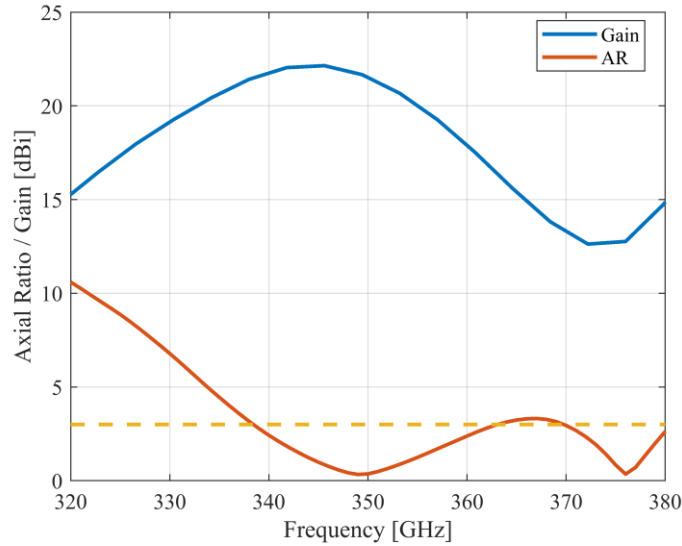
Figure 17. Axial ratio and gain plot in frequency for the θ = 0°, and β = 0°.
β describes the progressive phase shift.

5.4 SUMMARY

In this chapter, the complete design of high-gain, low profile 2×2 antenna element slot antenna arrays with corporate feed is presented. The principle of feeding, radiation and creation of circular polarization are presented. The instructions for designing and optimization of such design are given. The design of the expanded 4×4 array is described.

Two designed antenna arrays are in 2×2 and 4×4 configuration. The antennas operate with circular polarization at 350 GHz, have polarization and impedance bandwidths of 25 GHz and

30 GHz, with peak gains 13.8 dBi and 18.4 dBi, respectively. Antenna arrays have a low profile of only 1.3 λ_0.

The antennas performance is compared to other state-of-art designs. To author's knowledge, the presented design is the first antenna operating at THz frequency with simultaneously achieving such high gain, circular polarization, low-profile, wide bandwidth, and the possibility to extend to larger antenna arrays without significantly increasing the manufacturing/assembly complexity.

Moreover, the development of different full-wave models of a terahertz antenna array is discussed. The performances of the analyzed models in two commercial solvers are compared, and the best models for different applications are recommended. The parametric analyses of surface roughness and gold layer thickness are performed prior to manufacture. It is concluded that increasing surface roughness influences the radiation efficiency negatively and the gold layer thickness does not influence the antenna performance significantly. However, very thick gold can change the radiation pattern slightly.

The 8x8 antenna array with beam steering capabilities is presented. In the feeding layer of the designed antenna array, phase shifters were implemented. The antenna operates at 350 GHz with circular polarization. By introducing a progressive phase shift form -80° to 80° in the feeding layer, the beam can be steered from -8° to 8° in both the dimensions: elevation and azimuth. The gain of the antenna remains above 21 dBi for all the beam directions.

6 FABRICATION TECHNOLOGY AND MEASUREMENTS

In this chapter, the fabrication technology is discussed. The antennas designed in chapter 5 were manufactured in micromachining technology. All the steps are described in detail and photos of the samples during fabrication and final manufactured antennas are shown. The fabricated antennas are characterized by their reflection coefficients. The surface roughness measurements by Scanning Probe Microscope and Electron Microscope are presented.

6.1 MANUFACTURING TECHNOLOGY

The short description of the fabrication process is given here. The microfabrication steps are depicted in Figure 18.

- Prior to manufacture, elements necessary for the alignment of the layers of the antenna were added. Two big circles and three small circles were included in the design. Also, the size of each layer was enlarged to 1 cm ×1 cm for easier handling and mounting on the flange.

- Structures (slots, cavities and waveguides) were cut by a laser in a p-type, 200 µm thick, 2-inch silicon wafer. The average accuracy of the cut of structures was about 15 um.

- Wafers were diced into 1 cm × 1 cm samples. The samples after dicing are presented

in Figure 19.

- The 400 nm thick gold layer was evaporated on the samples. The samples were tilted by 15° and were being rotated during the evaporation to ensure that gold covers surfaces inside the cavities and slots. The samples mounted onto the rotation device are shown in Figure 20.

- Samples were bonded using silicon eutectic bonding, under 330° C and an average of 100 N pressure on a FineTech Flip Chip machine. Bonding was performed layer by layer. Each process lasted 55 minutes. The 4×4 and 2×2 arrays are shown in Figure 21.

- Copper patches on the top dielectric layer (Arlon CuClad217) were etched using a standard lithography process with a negative photoresist nLOF.

- A dielectric top layer was precisely aligned and glued to the antenna using the bonding machine without any heating. Figure 22 depicts the top view of the two of the manufactured antennas

- The antenna was attached to a flange.
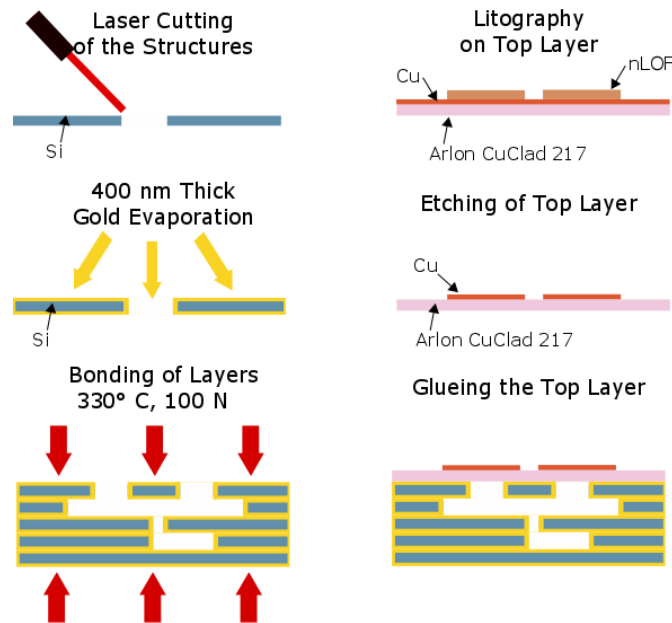
Figure 18. Microfabrication steps of the antennas.

Figure 19. Wafer with the 4x4 antenna array layers after dicing into samples.

Figure 20. Silicon samples on the holder before gold evaporation.
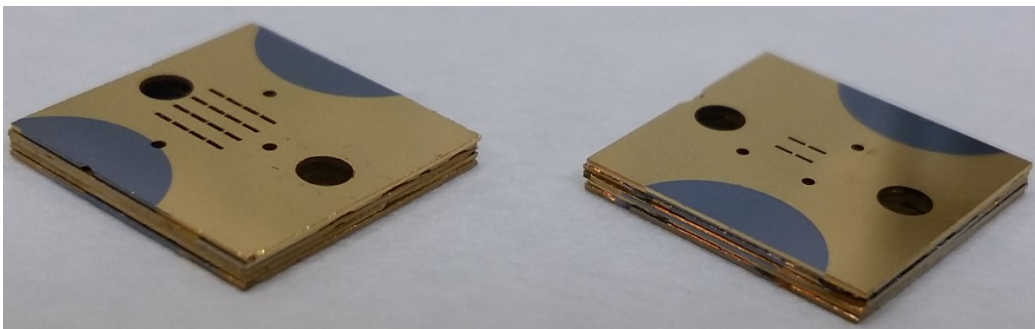
Figure 21. 4x4 and 2x2 antennas before mounting the top layer.
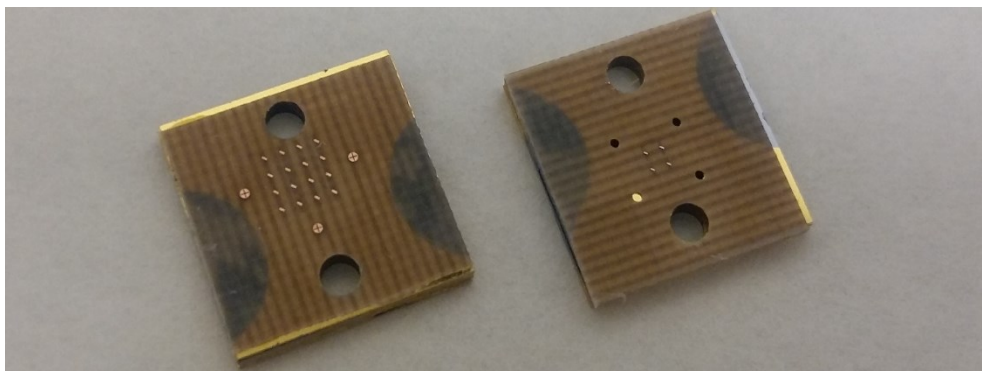
Figure 22. Manufactured 4x4 and 2x2 antenna arrays.

6.2   MEASUREMENTS

6.2.1 Reflection Coefficient Measurements

The manufactured antennas were connected to a VNA through a frequency extender through a stadard WR2.2 waveguide.

Two manufactured 2x2 antenna arrays and two manufactured 4x4 antenna arrays were connected to the VNA and their reflection coefficient was measured. In, the Figure 23 reflection coefficient of the two 2×2 antenna arrays is plotted together with the reflection coefficient from the simulation of this antenna. Deviations are due to manufacturing inaccuracies such as over-etching of the slots and cavities and high surface roughness, caused by laser cutting. Therefore, another simulation was added to the graph, taking manufacture inaccuracies into account (decreased conductivity, dimensions of slots and cavity varying within ±30 μm). The simulation with manufacture inaccuracies is similar to the measured results.

Figure 23. Measured frequency response of the reflection coefficient compared with the simulated one for the 2x2 antenna array.

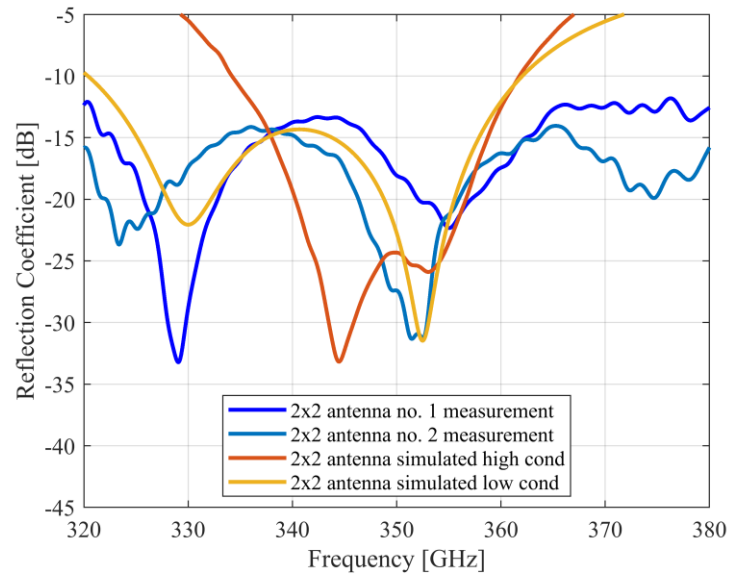## 6.2.2 Surface Roughness Measurements

To investigate the sources of deviations in the reflection coefficient measurement results the surface roughness was measured by a scanning probe microscope in CEITEC cleanroom. The profile of the tested surface without the elevated black rectangles is presented in Figure 24
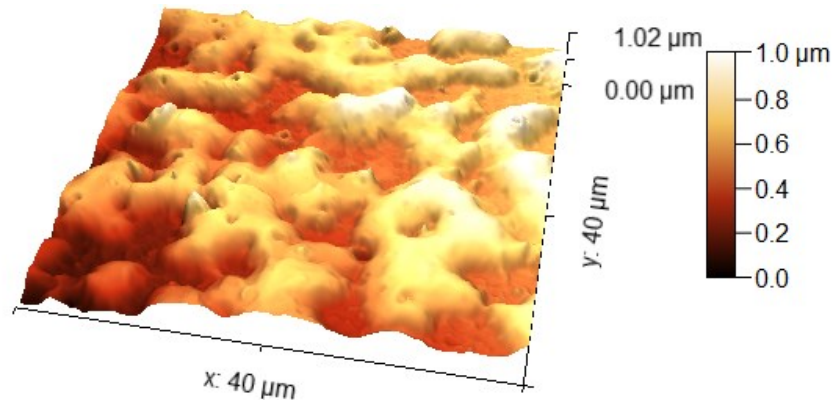
Figure 24. Surface roughness profile of 40 μm × 40 μm spot. Image prepared from measurement by Scanning Probe Microscope.

The average surface roughness (RMS) was calculated, from the measurements by Scanning Probe Microscope, to be 500 nm which is higher than the gold layer thickness on the antenna surface. Hence, the laser cutting caused the average value of the surface roughness to be as high as the thickness of the layer of the antenna. This roughness decreased the conductivity and introduced losses. Moreover, the inaccuracy of the cutting changed the sizes of the slots and cavities resulting in changed resonance and coupling parameters. In the future manufacture of the antenna, the laser cutting will be avoided. Instead, a deep reactive ion etching should be used.

6.3   SUMMARY

In this chapter, the microfabrication of the antenna is presented. Each step of the manufacturing including structures etching, wafer dicing, gold evaporation, bonding, dielectric layer fabrication and assembly are discussed in detail. The presented technology is cheaper and more available than traditional micromachining. Four antenna arrays were manufactured by the described technology.

The antenna performance is characterized by the reflection coefficient measurements conducted by a VNA. Deviations between the simulated results and the measured ones are obtained due to a lower surface roughness. Surface roughness was measured and included in the simulations to explain the deviations.

7   LOW-PROFILE ANTENNA FOR SPACE APPLICATIONS

In corporate feed, multilayer antenna arrays, radiating slots are fed with cavities and waveguides placed below them without any movable mechanical elements. Such a solid multilayer design results in a significant performance while maintaining a low-profile and reliable operation. Those qualities make the antenna a good fit for CubeSats communication links. In this chapter, a corporate feed, multilayer 8x8 antenna array operating with circular polarization at 35 GHz is presented. The antenna has a higher gain, a wider bandwidth, and much more compact size than state-of-art antennas demonstrated in [31] and [32].

7.1   DESIGN OF ANTENNA ARRAY AT 35 GHZ

7.1.1 Design of a 2×2 antenna element

The 2x2 antenna element from chapter 5 is scaled down to 35 GHz. The antenna consists of four metallic layers, with hollow waveguides, slots and cavities. The height of each metallic layer is 2 mm.

The antenna structure is completed by a dielectric layer with metallic patches. The dielectric layer of a height 1.27 mm is made from Arlon Cuclad 217 [38]. The E-bend was not included in the design of the 2×2 antenna for simplification.

The design was scaled. However the waveguide dimensions had to be selected to agree with the waveguide WR standards for the 35 GHz band. The WR-22 was chosen with the size 5.69 mm x 2.845 mm and the cut-off frequency 26.346 GHz. Some adjustments of the dimensions were made to achieve good results.

A 2×2 array element of the antenna was analyzed in CST Microwave Studio. The antenna is designed in a manner that enables expansion to a larger array. The reflection coefficient response in frequency has the minimum at 35 GHz and the bandwidth of 0.76 GHz.

7.2 PROTOTYPE AT 9 GHZ

As a proof of concept, a prototype of the 2×2 array was scaled down to a central frequency of 9 GHz and manufactured from polylactic acid (PLA) by the 3D printing technique. The printed structure was metalized by a nickel spray paint. This fabrication technology provides several benefits for prototyping such as rapid manufacturing, an efficient cost, and a lightweight.

At 9 GHz, it is easier to feed the antenna with a coaxial cable than a waveguide. Therefore, a transition from a coaxial connector to a waveguide was designed.

The antenna was manufactured in 4 pieces by the 3D printing in PLA. The functional surfaces of the PLA were metalized by a nickel spray. The patches were manufactured by a standard lithography process and glued to the top PLA layer. The dielectric permittivity of the PLA varies depending on the filling factor. Here, the permittivity was assumed to be 2.7 as measured in [42].

The manufactured antenna is presented in Figure 25.
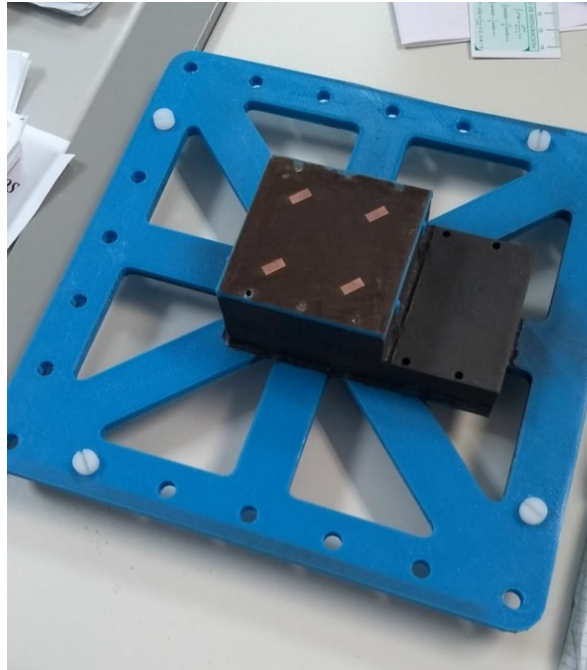
Figure 25. The 2x2 antenna prototype manufactured by 3D-printing.

7.2.1 Measurements

The simulated and measured reflection coefficients are shown in Figure 26. A small shift in

the resonance frequency (about 1.4 GHz) was observed. The reason for this behavior seems to be the problem with the manufacture which was further investigated.
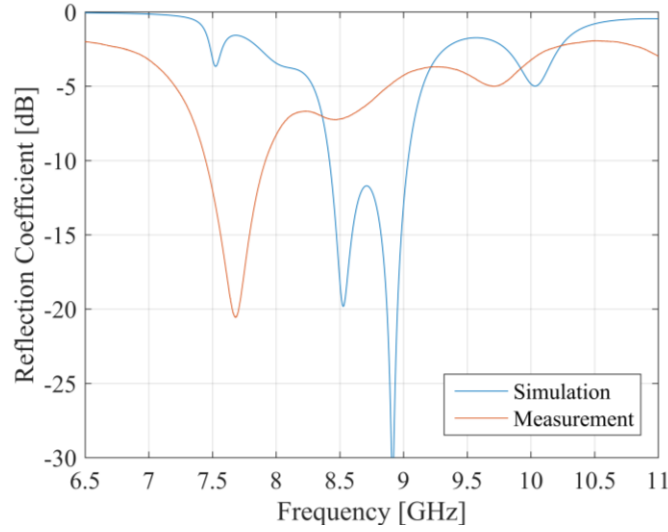

Figure 26. Measured and simulated reflection coefficient of the antenna prototype on 9 GHz.

Axial ratio curves were prepared based on the radiation pattern measurements and are presented in Figure 27. It can be noticed that the axial ratio minima is slightly shifted to the lower frequencies. The shift probably happened because of changes in the filling factor of the PLA which caused a change of its dielectric permittivity. This was not considered as a significant problem, because the top dielectric layer can be easily redesigned and manufactured again to accommodate these inaccuracies.
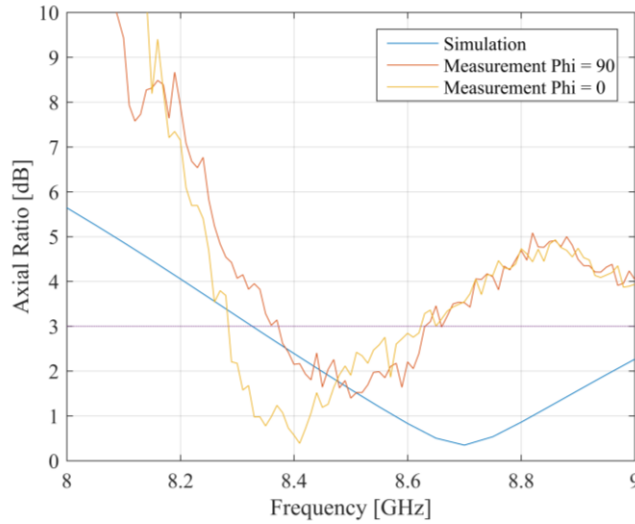
Figure 27. Measured and simulated axial ratio of the 9 GHz antenna.

The comparison of the measured and simulated radiation patterns is presented in Figure 28 and Figure 29 for different cut planes. Measured and simulated radiation patterns are in agreement and the measurements prove circular polarization operation of the antenna.

The minor discrepancies in the results occurred, however the prototype confirmed the overall impressive performance of this antenna design at 9 GHz.
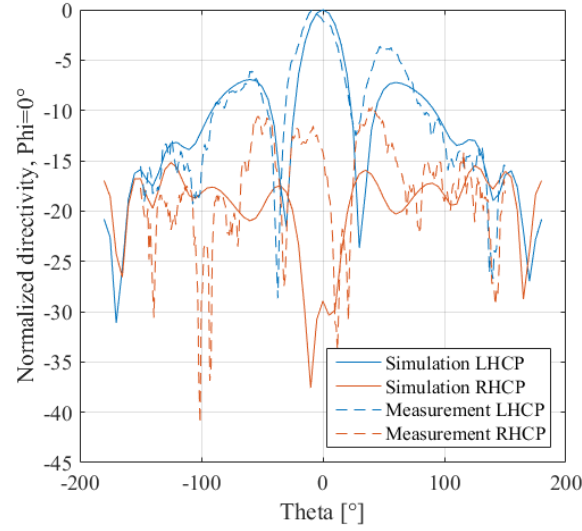
Figure 28. Comparison of the measured and simulated radiation pattern of the antenna prototype on 9 GHz, in the φ=0° plane.
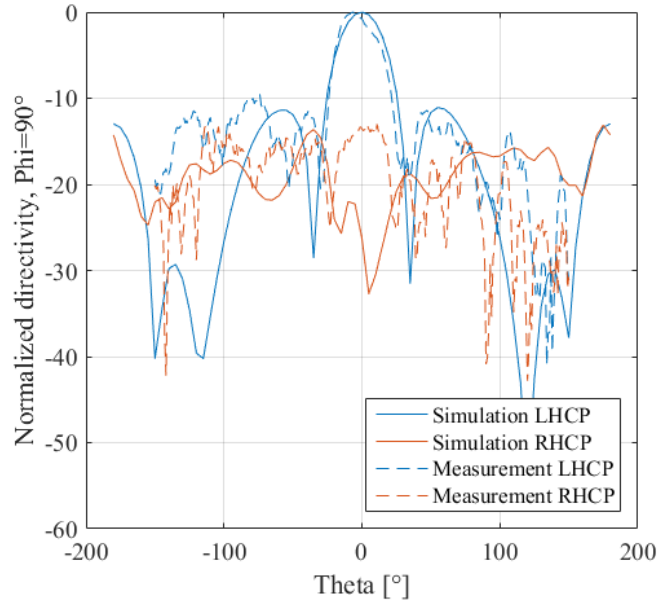
Figure 29. Comparison of the measured and simulated radiation pattern of the antenna prototype on 9 GHz, in the φ=90° plane

7.3   THE 8X8 ANTENNA ARRAY AT 35 GHZ

7.3.1 Antenna design

The 2×2 antenna was expanded into an 8×8 array. The antenna consists of five metallic layers, with hollow waveguides, slots and cavities and one dielectric layer with metallic patches. The 8x8 structure is corresponding to the 2x2 design presented in section 5.1.1. The array was expanded from 4 elements to 64 and the feeding system was added into the waveguide layer. The feeding layer consists of T and H shaped power dividers that guide and divide the signal equally to the coupling slots.

7.3.2 Simulation results

The central operation frequency of the antenna is 35 GHz with the impedance bandwidth and the axial ratio bandwidth of 1.1 GHz. The antenna achieves a peak gain of 26.5 dBi. The gain is over 26 dBi in the whole band. The gain and axial ratio plots are presented in Figure 30.

The radiation patterns of the antenna are shown in Figure 31. They present a co-polar / cross-polar level in broadside ($\theta = 0°$) greater than 25 dB with a front-to-back ratio higher than 35 dB. Parameters of the antenna array were optimized by the full-wave simulation in CST Microwave Studio.
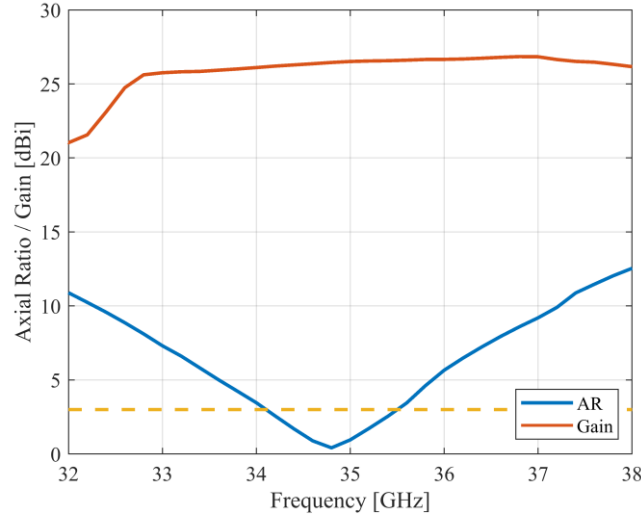
Figure 30. The 8x8 antenna array gain and axial ratio plotted in frequency.
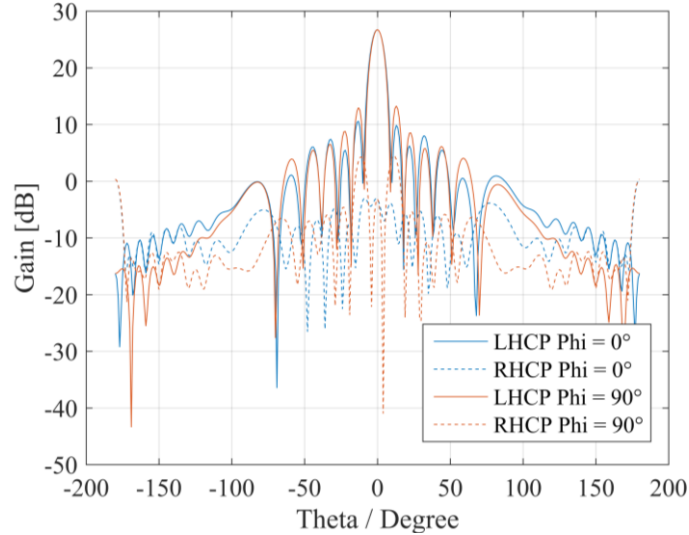
Figure 31. Radiation patterns in gain, $\theta = 0°$ and $\theta = 90°$, of the 8x8 antenna array at 35 GHz.

7.3.3 Manufacturing

The antenna was manufactured by CNC machining. However the results were not acceptable, a lot of inaccuracies were visible, and therefore another method was sought. The results of the

CNC drilling manufacture is presented in Figure 32.
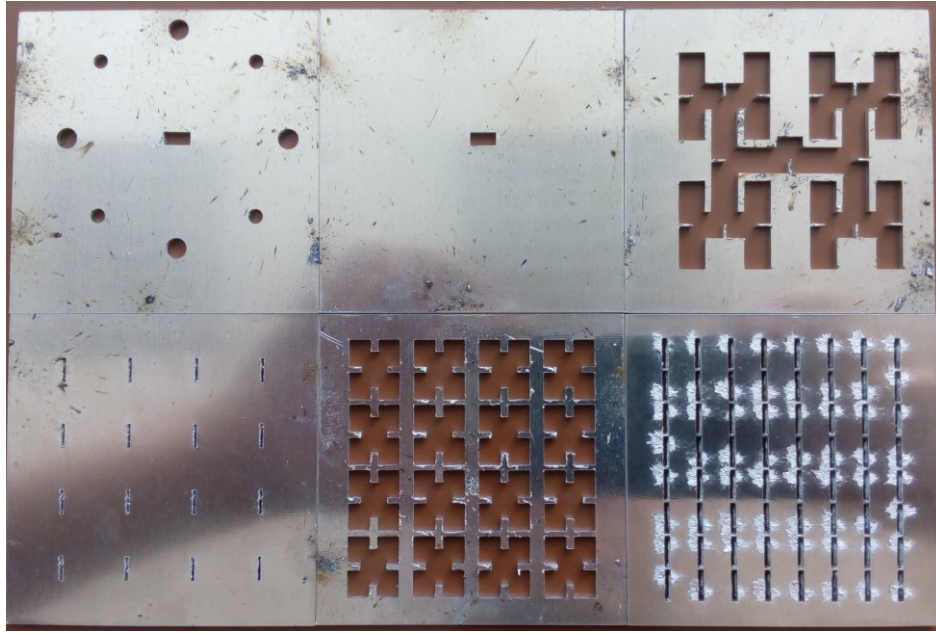
Figure 32. Results of the CNC machining antenna manufacturing.

The antenna was prepared for manufacture by wire cutting in the Penta company in Brno. Technical drawings of the antenna were prepared. Unfortunately because of unpredicted financial issues, the antenna could not be manufactured.

7.3.4 Comparisons with state of art

The designed antenna is compared with the state-of-art circularly polarized antenna designed for CubeSats [32]. The designed antenna size is 55 mm × 55 mm, which corresponds to a total area of 6×6 λ_0. This design is a more compact with an area of only 51% of the area of the antenna presented in [32]. The impedance bandwidth is 1.6% wider than in case of the antenna from [32].

The designed antenna has higher gain, higher co-polar to cross-polar level and much more compact size than state-of-art antennas demonstrated in [31] and [32]. The presented comparisons show that the antenna is a great fit for CubeSats applications.

7.4 SUMMARY

A circularly polarized 8x8 antenna array operating in Ka-band was designed with a peak gain of 26.5 dBi, 40 λ_0^2 size, and bandwidth of 1.1 GHz. The antenna provides a higher gain and a wider bandwidth with a more compact design compared to state-of-art antennas. This makes it a great fit for a communication antenna on a CubeSat.

A prototype of the antenna was manufactured with 3D printing at 9 GHz as a proof of the concept. A good agreement between the simulated and measured radiation patterns was found and circular polarization was confirmed.

8   CONCLUSIONS

The original contribution of this thesis lies in the area of high-gain circularly polarized THz antenna design, proper modeling of thin metallic structures at THz frequencies and a description of cheaper and more available manufacture technology. Moreover, the generality of the antenna design is proven by scaling down the antenna to a lower frequency.

Modeling of metal at THz frequencies was discussed in terms of the Drude model and different conductivity measurements. Comparison of modeling approaches for metallic structures was done and the best methods were selected based on the skin depth relation with metal thickness [43].

Circularly polarized corporate feed antenna array suitable for communications applications was designed. The antennas operate at 350 GHz with 2×2 and 4×4 element configuration. The designs include the possibility of extension to a larger array and take into consideration the fabrication possibilities at THz frequencies. The designed antenna arrays radiate waves with circular polarization, have polarization and impedance bandwidths of 25 GHz and 30 GHz, with peak gains 13.8 dBi and 18.4 dBi, respectively. Antenna arrays have a low profile of only 1.3 λ_0. According to the author's knowledge, the developed antennas are the first 350 GHz circularly polarized antennas with such high gain, wide bandwidth, low size and possibility to be easily extended to a larger array [43]. The designed 2×2 antenna element is analyzed by different methods and solvers and the best methods are recommended depending on the requirements [44].

The designed antenna array was expanded to an 8x8 antenna array with beam steering capabilities. The phase shifters were implemented in the feeding layer. The antenna radiates a highly directive beam with circular polarization. The beam steering is possible in two dimensions: horizon and elevation with the maximum steering capability from -8° to 8° with gain remaining above 21 dBi for all the beam directions. The designed antenna is an excellent fit for communications applications that require beam steering.

To fulfill the third objective, different manufacturing technologies were compared. The reactive ion etching was tested, however the laser cutting was eventually chosen to etch the structures. The 2×2 and 4×4 antenna arrays were manufactured in the microfabrication process. The manufacturing steps including etching, dicing, gold evaporation, bonding, lithography and assembly were described in detail [45]. The antenna reflection coefficient was measured and compared with simulations. Small discrepancies are associated with increased surface roughness of the layers. The surface roughness was measured by a scanning probe microscope and observed by scanning electron microscope and the assumptions were confirmed [43]. The radiation patterns of the antenna could not be measured because of the inability to find a suitably equipped laboratory in Europe. In order for European researchers to take the leading role in successful THz antenna design more well equipped clean rooms and measurement laboratories are necessary.

To verify the generality of the design, the THz antenna was scaled down to a Ka-band. The obtained circularly polarized 8x8 antenna array achieved a peak gain of 26.5 dBi, 7×7 λ_0 size, and bandwidth of 1.1 GHz. The antenna provides a higher gain with a more compact design compared to state-of-art antennas. This makes it a great fit for a communication antenna on a CubeSat. A prototype of the antenna was manufactured with 3D printing on 9 GHz as a proof of the concept. A good agreement between the simulated and measured radiation patterns was

found and circular polarization was confirmed [46].

Many interesting areas for future research open up based on the work presented in this dissertation thesis. Current commercial electromagnetic solvers do not deal well with simulating THz designs. Functionalities that allow to accurately account for possible manufacture inaccuracies, for example increased surface roughness, could be very beneficial for THz antenna designers.

In relation to chapter 5, the future research could include the designed antenna array extension to a larger array to further increase the gain. Furthermore, by removing the dielectric layer and instead including additional layer of oblique shaped slots. In such way, the whole antenna design can be implement fully in silicon substrate, while maintaining the circular polarization. To improve the manufacturing technology, deep reactive ion etching can be employed for smoother surface of the etched structures and lower losses related to the inaccuracies.

Another interesting research direction is passive phase shifters operating at THz frequencies. Not much work has been done in the field of passive phase shifters at this frequency range. Moreover, not only simulation, but actual implementation of liquid crystal or carbon nanotube based phase shifters in a THz antenna would be a novelty.

Dealing with chapter 7, further research should include fabrication and measurements of the designed antenna at 35 GHz to verify its usability for satellite communications such as CubeSats. Furthermore, beam steering can be implemented in the waveguides of the feeding system of the antenna, for example by including liquid crystal filled dielectric rod waveguides.

REFERENCES

[1]   K. R. Jha and G. Singh, *Terahertz Planar Antennas for Next Generation Communication*. Cham: Springer International Publishing, 2014.

[2]   I. Uchendu and J. R. Kelly, "Survey Of Beam Steering Techniques Available For Millimeter Wave Applications," *Prog. Electromagn. Res. B*, vol. 68, no. 1, pp. 35–54, 2016.

[3]   G. Maral and M. Bousquet, *Satellite Communications System Techniques and Technology*. Sussex, U.K.: John Wiley & Sons, Ltd., 2009.

[4]   F. E. Nathanson, *Radar design principles*, Second Edi. New Jersey: SciTech Publishing, Inc., 1991.

[5]   O. Malyuskin and V. Fusco, "Wideband circular polarised antenna with high polarisation purity over a wide angular range," in *2012 6th European Conference on Antennas and Propagation (EUCAP)*, 2012, pp. 2764–2765.

[6]   H. Maune *et al.*, "Liquid crystal technology for reconfigurable satcom applications," in *2017 Topical Workshop on Internet of Space (TWIOS)*, 2017, pp. 1–4.

[7]   D. V. Lioubtchenko, I. V. Anoshkin, I. I. Nefedova, J. Oberhammer, and A. V. Raisanen, "W-band phase shifter based on optimized optically controlled carbon nanotube layer," in *2017 IEEE MTT-S International Microwave Symposium (IMS)*, 2017, pp. 1188–1191.

[8]   D. Chicherin, M. Sterner, D. Lioubtchenko, J. Oberhammer, and A. V. Räisänen, "Analog-type millimeter-wave phase shifters based on MEMS tunable high-impedance surface and dielectric rod waveguide," *Int. J. Microw. Wirel. Technol.*, vol. 3, no. 5, pp. 533–538, Oct. 2011.

[9]   O. Kodheli *et al.*, "Satellite Communications in the New Space Era: A Survey and Future Challenges," *IEEE Commun. Surv. Tutorials, Prepr.*, pp. 1–45, Feb. 2020.

[10]   K. Pitra, Z. Raida, and J. Lacik, "Low-profile circularly polarized antenna exploiting fabry-perot resonator principle," *Radioengineering*, vol. 24, no. 4, pp. 898–905, 2015.

[11]   B. A. Zeb and K. P. Esselle, "A partially reflecting surface with polarization conversion for circularly polarized antennas with high directivity," in *2012 International Conference on Electromagnetics in Advanced Applications*, 2012, pp. 466–469.

[12]   R. Orr, G. Goussetis, and V. Fusco, "Design method for circularly polarized fabry-perot cavity antennas," *IEEE Trans. Antennas Propag.*, vol. 62, no. 1, pp. 19–26, 2014.

[13]   E. García-Muñoz *et al.*, "Photonic-based integrated sources and antenna arrays for broadband wireless links in terahertz communications," *Semicond. Sci. Technol.*, vol. 34, no. 5, p. 54001, 2019.

[14]   W. Hou, Z. Sun, Y. Jiang, Y. Liu, and X. Lv, "A terahertz diagonal multi-layer horn antenna based on MEMS technology," in *2015 IEEE MTT-S International Microwave Workshop Series on Advanced Materials and Processes for RF and THz Applications (IMWS-AMP)*, 2015, pp. 1–3.

[15]   A. Rivera-Lavado *et al.*, "Planar Lens–Based Ultra-Wideband Dielectric Rod Waveguide Antenna for Tunable THz and Sub-THz Photomixer Sources," *J. Infrared, Millimeter, Terahertz Waves*, vol. 40, no. 8, pp. 838–855, Aug. 2019.

[16]   A. Rivera-Lavado *et al.*, "Design of a Dielectric Rod Waveguide Antenna Array for Millimeter Waves," *J. Infrared, Millimeter, Terahertz Waves*, vol. 38, no. 1, pp. 33–46, Jan. 2017.

[17] M. Geiger, M. Hitzler, and C. Waldschmidt, "A flexible dielectric leaky-wave antenna at 160 GHz," in *2017 47th European Microwave Conference (EuMC)*, 2017, vol. 2017-Janua, pp. 240–243.

[18] D. Kim, J. Hirokawa, M. Ando, J. Takeuchi, and A. Hirata, "64 × 64-element and 32 × 32-element slot array antennas using double-layer hollow-waveguide corporate-feed in the 120 GHz band," *IEEE Trans. Antennas Propag.*, vol. 62, no. 3, pp. 1507–1512, 2014.

[19] K. M. Luk *et al.*, "A microfabricated low-profile wideband antenna array for terahertz communications," *Sci. Rep.*, vol. 7, no. 1, pp. 1–11, 2017.

[20] K. Tekkouk *et al.*, "Corporate-feed slotted waveguide array antenna in the 350-GHz band by silicon process," *IEEE Trans. Antennas Propag.*, vol. 65, no. 1, pp. 217–225, 2017.

[21] J. Hirokawa, T. Tomura, Y. Miura, M. Zhang, and M. Ando, "Plate-laminated-waveguide corporate-feed slot array antennas with a polarization conversion layer," in *2011 IEEE MTT-S International Microwave Workshop Series on Millimeter Wave Integration Technologies*, 2011, pp. 29–32.

[22] P. Lu *et al.*, "Photonic Integrated Chips for Millimeter-Wave and THz Beam Steering Antennas," in *2019 21st International Conference on Transparent Optical Networks (ICTON)*, 2019, pp. 1–4.

[23] A. Gomez-Torrent *et al.*, "A Low-Profile and High-Gain Frequency Beam Steering Subterahertz Antenna Enabled by Silicon Micromachining," *IEEE Trans. Antennas Propag.*, vol. 68, no. 2, pp. 672–682, 2020.

[24] K. Sarabandi, A. Jam, M. Vahidpour, and J. East, "A Novel Frequency Beam-Steering Antenna Array for Submillimeter-Wave Applications," *IEEE Trans. Terahertz Sci. Technol.*, vol. 8, no. 6, pp. 654–665, 2018.

[25] H. Jalili and O. Momeni, "Scalable wideband and wide-angle beam steering mm-wave/THz radiator and phased arrays in silicon," in *Asia-Pacific Microwave Conference Proceedings, APMC*, 2019, vol. 2018-Novem, pp. 1157–1159.

[26] S. Rey, T. Merkle, A. Tessmann, and T. Kurner, "A phased array antenna with horn elements for 300 GHz communications," in *ISAP 2016 - International Symposium on Antennas and Propagation*, 2017, pp. 122–123.

[27] R. Reese *et al.*, "Liquid crystal based dielectric waveguide phase shifters for phased arrays at W-band," *IEEE Access*, vol. 7, pp. 127032–127041, 2019.

[28] W. Fuscaldo *et al.*, "A reconfigurable multilayered THz leaky-wave antenna employing liquid crystals," in *2017 11th European Conference on Antennas and Propagation, EUCAP 2017*, 2017, pp. 849–851.

[29] N. Chahat *et al.*, "CubeSat Deployable Ka-Band Mesh Reflector Antenna Development for Earth Science Missions," *IEEE Trans. Antennas Propag.*, vol. 64, no. 6, pp. 2083–2093, 2016.

[30] C. Han, J. Huang, and K. Chang, "A high efficiency offset-fed X/Ka-dual-band reflectarray using thin membranes," *IEEE Trans. Antennas Propag.*, vol. 53, no. 9, pp. 2792–2798, 2005.

[31] J. Che *et al.*, "6 GHz to 40 GHz CubeSat Radiometer Antenna System," *IEEE Trans. Antennas Propag.*, vol. 67, no. 5, pp. 3410–3415, 2019.

[32] D. Gonzalez Ovejero, X. Morvan, N. Chahat, G. Chattopadhyay, R. Sauleau, and M. Ettorre, "Metallic Metasurface Antennas for Space," in *12th European Conference on Antennas and Propagation (EuCAP 2018)*, 2018, no. 1, pp. 372–372.

[33]   R. Ghodssi and P. Lin, Eds., *MEMS Materials and Processes Handbook*, vol. 1. Boston, MA: Springer US, 2011.

[34]   H. V. Jansen, M. J. De Boer, S. Unnikrishnan, M. C. Louwerse, and M. C. Elwenspoek, "Black silicon method X: A review on high speed and selective plasma etching of silicon with profile control: An in-depth comparison between Bosch and cryostat DRIE processes as a roadmap to next generation equipment," *J. Micromechanics Microengineering*, vol. 19, no. 3, 2009.

[35]   M. D. Henry, C. Welch, and A. Scherer, "Techniques of cryogenic reactive ion etching in silicon for fabrication of sensors," *J. Vac. Sci. Technol. A Vacuum, Surfaces, Film.*, vol. 27, no. 5, pp. 1211–1216, 2009.

[36]   R. Dussart, T. Tillocher, P. Lefaucheux, and M. Boufnichel, "Plasma cryogenic etching of silicon: From the early days to today's advanced technologies," *J. Phys. D. Appl. Phys.*, vol. 47, no. 12, 2014.

[37]   A. Berenguer, M. Baquero-Escudero, D. Sanchez-Escuderos, and F. Vico, "Rigorous method for calculating Gap waveguides impedance using transmission line theory," in *8th European Conference on Antennas and Propagation EuCAP*, 2014, pp. 2508–2512.

[38]   Rogers, "CuClad Series ® PTFE / Woven Fiberglass Laminates Typical Properties." [Online]. Available: https://rogerscorp.com/-/media/project/rogerscorp/documents/advanced-connectivity-solutions/english/data-sheets/cuclad-laminates-data-sheet.pdf.

[39]   A. Mir and J. Yu, "Broadband circular polarized cross bow tie antenna for terahertz range," in *2014 IEEE Antennas and Propagation Society International Symposium (APSURSI)*, 2014, pp. 416–417.

[40]   C. Lee *et al.*, "Terahertz antenna arrays with silicon micromachined-based microlens antenna and corrugated horns," in *2015 International Workshop on Antenna Technology (iWAT)*, 2015, pp. 70–73.

[41]   K. A. Abdalmalak *et al.*, "Ultrawideband Conical Log-Spiral Circularly Polarized Feed for Radio Astronomy," *IEEE Trans. Antennas Propag.*, vol. 68, no. 3, pp. 1995–2007, 2020.

[42]   S. Zhang, C. C. Njoku, W. G. Whittow, and J. C. Vardaxoglou, "Novel 3D printed synthetic dielectric substrates," *Microw. Opt. Technol. Lett.*, vol. 57, no. 10, pp. 2344–2346, Oct. 2015.

[43]   D. Warmowska, K. A. Abdalmalak, L. E. G. Munoz, and Z. Raida, "High-gain, Circularly-polarized THz Antenna with Proper Modeling of Structures with Thin Metallic Walls," *IEEE Access*, pp. 1–1, 2020.

[44]   D. Warmowska and Z. Raida, "High-Gain Circularly Polarized Corporate-Feed Terahertz Antenna Array," *Proc. 2018 20th Int. Conf. Electromagn. Adv. Appl. ICEAA 2018*, pp. 157–160, 2018.

[45]   D. Warmowska and Z. Raida, "Manufacture of a Corporate-Feed Multilayer Terahertz Antenna Array in Silicon Technology," in *Asia-Pacific Microwave Conference Proceedings, APMC 2019*, pp. 1–2.

[46]   D. Warmowska, K. A. Abdalmalak, L. E. G. Munoz, and Z. Raida, "A Compact Circularly Polarized High-Gain Antenna Array for Ka-Band CubeSats Applications," in *2019 IEEE-APS Topical Conference on Antennas and Propagation in Wireless Communications (APWC)*, 2019, pp. 178–180.

CURRICULUM VITAE

DOMINIKA WARMOWSKA

Date of birth: 25 February 1992
Nationality: Polish
E-mail: Dominika.Warmowska@gmail.com
Phone: +420 608 125 251

EDUCATION

2016.10 - current **Brno University of Technology**
Ph.D. candidate
Thesis subject: THz antenna arrays

2015.02 - 2016.08 **Gdańsk University of Technology**
Msc.: Electronics and Telecommunications

2011.10 - 2015.02 **Gdańsk University of Technology**
Bsc.: Electronics and Telecommunications

RESEARCH STAYS

2018.09 - 2019.01 **Technical University of Darmstadt**
2018.04 - 2019.05 Work in a cleanroom. Micro- and nano- fabrication technologies. Studies on plasma etching, gold evaporation and silicon bonding.

2018.04 - 2018.05 **Carlos the Third University in Madrid**
2019.03 - 2019.04 Work on a high gain, low profile, circularly polarized antenna array suitable for CubeSats and space applications.

2017.10 - 2018.01 **KTH Royal Institute of Technology in Stockholm**
Studies about micromachining technology, dielectric waveguides and waveguide slot antennas.

WORK EXPERIENCE

2016.10 - 2019.10 **Convergence of Electronics and Photonics Technologies for Enabling Terahertz Applications (CELTA)**
Early Stage Researcher, Marie Skłodowska-Curie scholarship beneficiary
International collaboration in order to utilize Terahertz technology for

applications for sensing, instrumentation, imaging, spectroscopy, and communications.

2014.07 - 2014.09   **Powel AS Norway**
Intern in the Strategy and Technology Department
Developing a strategic plan for a new product that Powel was to introduce, conducting market research, analyzing existing solutions, customizing the software to a suitable demo case, developing a user-friendly interface, evaluating success criteria.

2014.06 - 2014.07   **PIT RADWAR**
Intern in the Analog Technologies Department
Designing parts of radiolocation systems, modeling and simulating passive elements, measuring characteristics of antennas, analyzing the outcomes.

2011.11 - 2014.06   **Board of European Students of Technology**
Member of the local group and International Financial Team
Teamwork in organizing local and international student events. Managing finances of the international organization, various soft-skills trainings.

ABSTRACT

The thesis is focused on the research of THz antenna arrays to be used for communications. Attention is turned to modeling metallic surfaces at THz frequencies, a proper characterization of gold conductivity, its relation to Drude model and corresponding measurements. Moreover, the best methods for modeling thin metallic layers (depending on the skin depth related to the metal thickness) are presented.

An optimized element of a THz 2×2 antenna array designed for the application of communications is developed in a way that enables an expansion to a larger array. The expansion ability is demonstrated on a 4×4 antenna array which is presented in the thesis too. The designed antennas achieve parameters better than the state-of-art antennas. The presented antennas radiate circularly polarized wave at THz frequencies, operate in a wide bandwidth, have a high gain and are of a compact size.

In the thesis, an 8×8 antenna array with a beam steering capability is presented. The main beam of the antenna array can be controlled in two dimensions. A high gain of the radiated circularly-polarized wave can be achieved that way.

Different approaches to modeling antennas with thin metallic layers are compared and the best methods are recommended from the viewpoint of different requirements. The designed 2×2 and 4×4 antenna arrays are manufactured using a microfabrication technology. Each step of the fabrication is described in detail and discussed. The reflection coefficient at the input of antennas is measured and compared with simulations. Discrepancies in results are associated with surface roughness which is analyzed by a scanning probe microscope and a scanning electron microscope.

By down-scaling the developed THz antenna, a low-profile high-gain antenna for Ka-band space applications is designed. The presented antenna achieves better results than state-of-art CubeSat antennas. The antenna performance is verified by a prototype to be operated at 9 GHz, and the radiation characteristics are experimentally confirmed.